Article

Neuron

Glycinergic Inhibitory Plasticity in Binaural Neurons Is Cumulative and Gated by Developmental Changes in Action Potential Backpropagation

Highlights

- Inhibitory glycinergic inputs to MSO neurons undergo long-term potentiation
- iLTP requires NMDAR-mediated calcium influx and action potential firing
- iLTP is proportional to stimulus frequency and number but not fine-scale timing
- iLTP is gated developmentally by reductions in action potential backpropagation

Authors

Bradley D. Winters, Nace L. Golding

Correspondence

golding@austin.utexas.edu

In Brief

Winters et al. demonstrate a mechanism for reinforcement of inhibitory inputs that are coactive with excitatory inputs in a brainstem circuit critical for sound localization, and this plasticity is gated developmentally by the progressive decline of action potential backpropagation.

Winters & Golding, 2018, Neuron *98*, 166–178
April 4, 2018
https://doi.org/10.1016/j.neuron.2018.03.001

CellPress

CellPress

Neuron
Article

Glycinergic Inhibitory Plasticity in Binaural Neurons Is Cumulative and Gated by Developmental Changes in Action Potential Backpropagation

Bradley D. Winters[1] and Nace L. Golding[1,2,*]
[1]The University of Texas at Austin, Department of Neuroscience and Center for Learning and Memory, 1 University Station C7000, Austin TX 78712-0248, USA
[2]Lead Contact
*Correspondence: golding@austin.utexas.edu
https://doi.org/10.1016/j.neuron.2018.03.001

SUMMARY

Utilization of timing-based sound localization cues by neurons in the medial superior olive (MSO) depends critically on glycinergic inhibitory inputs. After hearing onset, the strength and subcellular location of these inhibitory inputs are dramatically altered, but the cellular processes underlying this experience-dependent refinement are unknown. Here we reveal a form of inhibitory long-term potentiation (iLTP) in MSO neurons that is dependent on spiking and synaptic activation but is not affected by their fine-scale relative timing at higher frequencies prevalent in auditory circuits. We find that iLTP reinforces inhibitory inputs coactive with binaural excitation in a cumulative manner, likely well suited for networks featuring persistent high-frequency activity. We also show that a steep drop in action potential size and backpropagation limits induction of iLTP to the first 2 weeks of hearing. These intrinsic changes would deprive more distal inhibitory synapses of reinforcement, conceivably establishing the mature, soma-biased pattern of inhibition.

INTRODUCTION

The relative timing between synaptic inputs and action potential (AP) firing often controls the magnitude and direction of synaptic plasticity. Invasion of the dendrites by distally propagating APs (backpropagating action potentials, or BPAPs) can trigger local calcium influx and long-term plasticity at excitatory and inhibitory synapses that were active just prior to the spike, a process termed spike-timing-dependent plasticity (STDP). STDP thus communicates the output state of the neuron to the synapse.

For both excitatory and inhibitory synapses, spike timing-based learning rules rest on the assumption that the frequency of synaptic inputs is relatively low, imparting an unambiguous phase relationship between BPAPs, ongoing synaptic input, and the signal transduction cascades employed. Indeed, at cortical and hippocampal levels, where STDP is well established (Feldman, 2012; Vogels et al., 2013), the rules underlying synaptic plasticity appear to depend closely on the pattern of stimulation on a timescale of tens of milliseconds (Sjöström et al., 2001). What then are the rules that govern synaptic plasticity in the many neuron types in the brain that code information at much shorter timescales?

We examine this question at inhibitory synapses onto neurons of the medial superior olive (MSO), which enable horizontal sound localization by detecting microsecond differences in the arrival of sounds at the two ears (Goldberg and Brown, 1969; Pecka et al., 2008; Spitzer and Semple, 1995; Yin and Chan, 1990). Due to the unusually high requirement for precision in this computation, there has been intense interest in understanding how synaptic plasticity can optimize the organization and strength of the underlying circuitry (Gerstner et al., 1996). Inhibitory inputs to MSO neurons arise from the medial and lateral nuclei of the trapezoid body (MNTB and LNTB), modifying binaural information before it is transmitted to higher auditory centers (Cant and Hyson, 1992; Lorteije et al., 2009; Mc Laughlin et al., 2008; Recio-Spinoso, 2012; Roberts et al., 2014; Smith et al., 1991; Spirou et al., 1990). Inhibition, like excitation, is time locked to sub-millisecond precision with auditory stimuli and plays a critical role in sharpening the spatial receptive fields of MSO neurons (Brand et al., 2002; Pecka et al., 2008; Roberts et al., 2014). Inhibition is also coordinated in time with excitation in the MSO (Franken et al., 2015; Grothe and Sanes, 1993, 1994; Roberts et al., 2013).

Inhibitory synaptic inputs to MSO neurons undergo dramatic synaptic and structural refinements during auditory development. Prior to hearing onset, around postnatal day 12 (P12) in gerbils (McFadden et al., 1996), supernumerary synaptic inputs are distributed over the dendrites and soma but are extensively pruned during the succeeding 2 weeks of hearing, ultimately leaving synapses from only 2 to 4 powerful fibers that are temporally correlated with excitation and are concentrated at the soma and proximal dendrites (Clark, 1969; Couchman et al., 2010; Franken et al., 2015; Kapfer et al., 2002; Magnusson et al., 2005; Perkins, 1973; Rautenberg et al., 2009; Roberts et al., 2013; Werthat et al., 2008). The segregation of inhibition to the soma is experience dependent and is disrupted by deafening and noise rearing (Kapfer et al., 2002; Werthat et al., 2008), but the rules underlying such striking synaptic and structural changes are not understood.

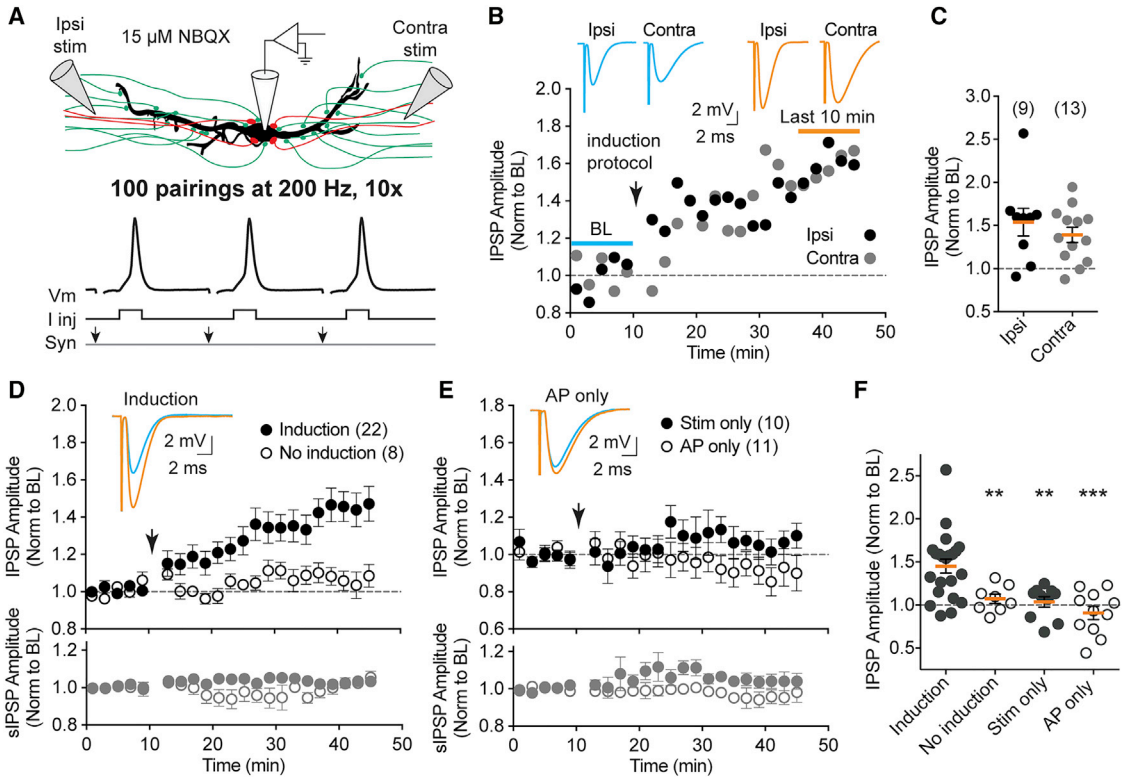

Figure 1. Trains of Coordinated AP Firing and Synaptic Stimulation Induces iLTP

(A) Diagram showing the typical recording and stimulation electrode placement during the induction protocol and a small portion of the induction train (Vm) with the simultaneous current injections (I inj) and dual synaptic stimulations (Syn).

(B) Example IPSP data in 2 min bins from a contralateral and an ipsilateral recording. Inset traces showing averages of all IPSPs for the baseline period (blue) and for the last 10 min (orange). Gray dashed line is at Y = 1 (no change).

(C) Last 10 min averages of all recordings divided into ipsilateral (LNTB) and contralateral (MNTB) stimulation location.

(D) Group data for cells that received paired stimuli (filled) and unstimulated controls (open) above and simulated IPSP measurements used to monitor cell stability below. Inset: average IPSP traces from one cell that received the induction protocol showing the 10 min baseline (blue) and last 10 min (orange).

(E) Group data showing that neither bilateral electrical stimulation of afferent fibers alone (filled) nor suprathreshold current injections alone (open) during induction produced potentiation.

(F) Last 10 min averages of all recordings shown in (D) and (E). Animal ages P12–P15 (13.5 average). Error ± SEM. **p ≤ 0.01; ***p ≤ 0.001.

Here we describe a form of inhibitory long-term potentiation (iLTP) at glycinergic synapses onto MSO neurons, from Mongolian gerbils, that functions at higher frequencies common in the auditory system and depends on the number and frequency of coactivations of inhibitory and excitatory inputs with APs, but in contrast to STDP is largely insensitive to their relative phase at these higher frequencies. This plasticity depends on postsynaptic N-methyl D-aspartate receptor (NMDAR) activation and calcium entry. We also find that the developmental reduction of the amplitude of BPAPs in the soma and dendrites over the first 2 weeks of hearing imposes a discrete developmental window for iLTP. These results reveal an intriguing interplay between the development of intrinsic membrane and voltage-gated ion channels properties and synaptic refinement in the MSO.

RESULTS

To understand how the emergence of sound-driven activity just after the onset of hearing affects the strength of inhibitory synapses in MSO neurons, we made whole-cell current-clamp recordings from MSO neurons in slices of gerbil brainstem (P12–P15, average P13.5), maintained the cells at –60 mV, and alternately activated ipsilateral and contralateral IPSPs that were isolated from fast excitation by bath applying 15 μM NBQX or in some cases CNQX to block amino-3-hydroxy-5-methyl-4 isoxazole propionic acid receptors (AMPARs, Figure 1A). Slower excitatory responses mediated by NMDARs were left unblocked, but when occasionally visible in younger animals were too slow to affect the peaks of IPSPs. After establishing a stable 10-min baseline at 0.1 Hz, we delivered a plasticity induction protocol consisting of trains of co-activated ipsilateral and contralateral synaptic stimulation with APs elicited by brief current pulses (100 stimuli at 200 Hz, repeated 10 times at an interval of 10 s, Figures 1A and 1B). This protocol is consistent with the high-frequency firing rates observed in excitatory inputs to the MSO from spherical bushy cells in the cochlear nucleus (Dehmel et al., 2010; Joris et al., 1994; Kuenzel et al., 2011) and the maximal firing rates of MSO neurons themselves (Brand et al., 2002; Franken et al.,

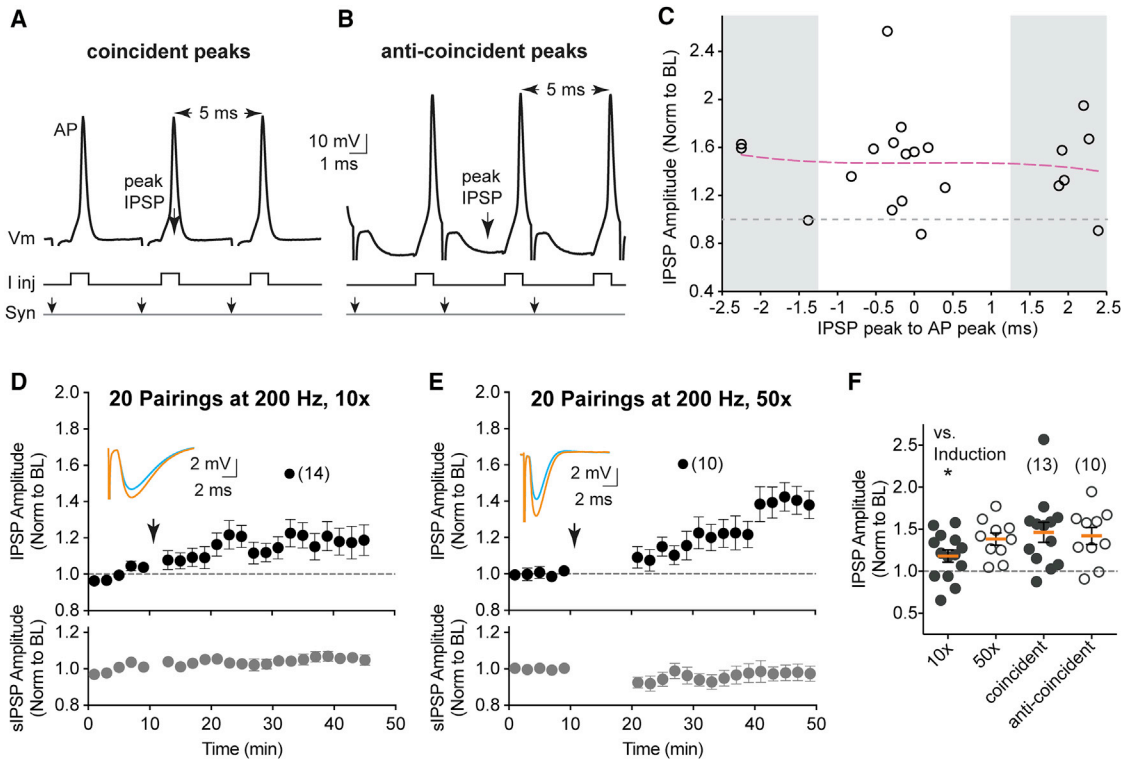

Figure 2. iLTP Is Insensitive to the Relative Timing of Stimuli at 200 Hz but depends on the Total Number of Pairings

(A and B) Diagrams showing a typical small portion of the induction train (Vm) and the timing of bilateral electrical stimulation (Syn) and current injections (I inj) for an experiment with (A) coincident IPSP and AP peaks and (B) anti-coincident peaks. Stimulation artifacts clipped for clarity.

(C) Last 10 min averages of all recordings in Figure 1F induction group plotted against the relative timing of the IPSP peak and AP peak during the induction protocol trains (magenta, cubic fit, $R^2 = 0.0075$).

(D and E) While 200 Hz induction trains with 100 pairings per train repeated 10 times effectively induced iLTP, induction trains with only 20 pairings repeated 10 times (D) were ineffective. Increasing the number of repetitions of the 20 pairing trains to 50 (E) recovered iLTP. Insets: average IPSP traces from one cell.

(F) Last 10 min averages for recordings shown in (C)–(E). Significance relative to the Induction group from Figure 1F. Animal ages P12–P15 (13.5 average). Error ± SEM. *$p \leq 0.05$.

2015; Goldberg and Brown, 1969; Yin and Chan, 1990). Additionally, MSO neuron excitatory inputs are able to drive 200 Hz firing at the ages examined (Figure S1). Separately evoked ipsilateral and contralateral IPSPs were then monitored again at 0.1 Hz for at least 34 min following the end of the induction protocol.

There was no difference in iLTP magnitude between ipsilateral inputs from the LNTB and contralateral inputs from the MNTB averaged between 24 and 34 min after the induction stimulus (Figures 1B and 1C: Ipsi, 1.54 ± 0.16, n = 9; Contra, 1.39 ± 0.09, n = 13; p = 0.388). Thus, the results for these independent sets of inputs, often measured in the same MSO neurons, were pooled for all experiments. The induction protocol increased IPSP amplitude by 45%, whereas omission of both induction stimuli resulted in no increase (Figures 1D and 1F: induction, 1.45 ± 0.08, n = 22, 11 gerbils; no induction, 1.07 ± 0.05, n = 8, 4 gerbils; p = 0.012). The average baseline IPSP amplitude was −4.09 ± 0.48 mV and there was no effect of IPSP amplitude on iLTP magnitude (Figure S2). Such stimuli activated substantial populations of excitatory inputs: in separate experiments, stimulation intensities that elicited IPSPs comparable to those in iLTP experiments consistently recruited suprathreshold excitation upon washout of AMPA receptor blockade. The stimulation threshold for excitatory fiber recruitment was an order of magnitude lower than that for inhibition (Figure S3). Neither APs nor electrical stimulation alone was sufficient to induce iLTP, indicating that cooperativity between synaptic input and AP firing was required for this form of plasticity (Figures 1E and 1F: AP only, 0.91 ± 0.08, n = 11, 3 gerbils, p = 0.0002 versus induction, p = 0.128 versus no induction; stim only, 1.04 ± 0.06, n = 10, 4 gerbils, p = 0.003 versus induction, p = 0.670 versus no induction).

In these experiments, there was no clear dependence of iLTP on the phase of IPSPs with respect to AP timing (Figures 2A–2C). Variations in the peaks of IPSPs and APs during the induction protocol, no matter whether induced explicitly by the experimenter or due to natural differences in synaptic delay, IPSP kinetics, and membrane time constants led to a range of relative phases of the paired stimuli. We found that iLTP was insensitive to the relative timing of the peak of the IPSP, measured in the absence of the AP, and the peak of the AP during the induction protocol (Figure 2C). There were no significant

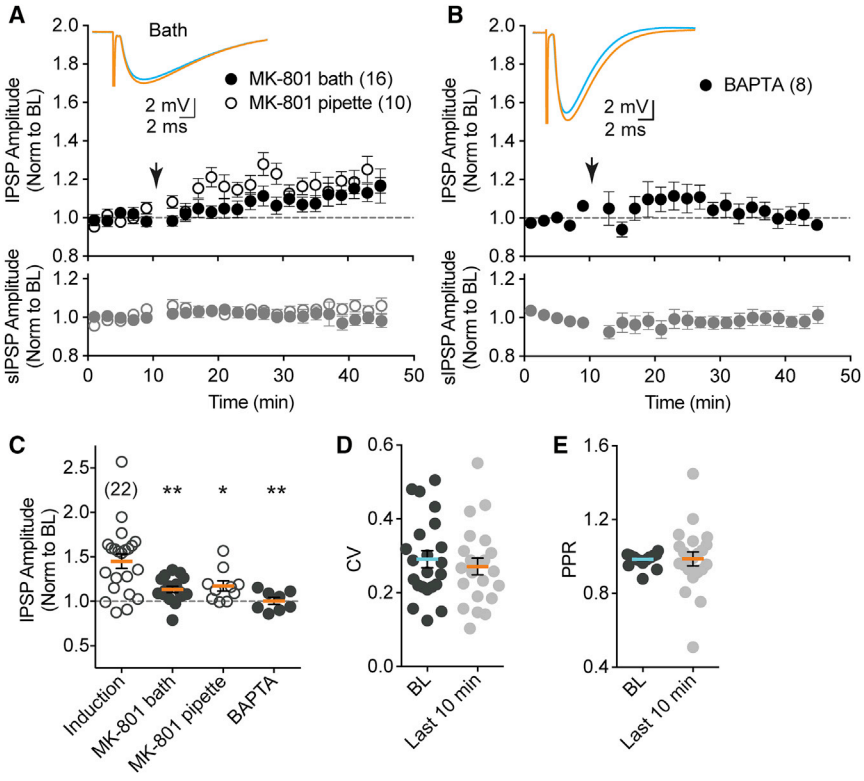

Figure 3. iLTP Requires Postsynaptic NMDA Receptor Activation and Calcium Dynamics

(A) Group data showing iLTP block by the use-dependent NMDAR blocker MK-801 in the bath (30 μM, filled) and in the recording pipette (1 mM, open). Inset: average IPSP traces from one cell that received bath application for the 10 min baseline (blue) and last 10 min (orange).

(B) Group data showing iLTP block by the Ca^{2+} chelator BAPTA in the recording pipette (15.9 mM). Inset: average IPSP traces from one cell.

(C) Last 10 min averages for recordings shown in (A) and (B), significance relative to the induction group from Figure 1F.

(D) The coefficient of variation for IPSP amplitudes from the induction group in Figure 1F was not altered by iLTP.

(E) The paired-pulse ratio (30 ms separation, P2/P1) of the IPSPs from the induction group in Figure 1F was also not altered by iLTP. Animal ages P12–P15 (13.5 average). Error ± SEM. *$p \leq 0.05$; **$p \leq 0.01$.

differences between experiments separated into coincident and anti-coincident groups consisting of IPSP-AP timing differences of –1.25 to 1.25 and >1.25 and <−1.25, respectively (Figures 2C and 2F: coincident pairing, 1.46 ± 0.12, n = 13; anti-coincident pairing, 1.44 ± 0.11, n = 9; p = 0.872). While iLTP induction appeared insensitive to the temporal fine structure of induction stimuli at such high frequencies, it did depend on the total number of pairings. Reducing the number of pairings in each induction train from 100 to 20 significantly reduced the effectiveness of iLTP induction protocols (Figures 2D and 2F: 1.18 ± 0.07, n = 14, 5 gerbils, p = 0.029 versus induction, p = 0.321 versus no induction). However, if the number of train repetitions was increased to provide the same 1,000 pairings as our standard iLTP protocol (in shorter bursts) the effectiveness was largely recovered (Figures 2E and 2F: 1.38 ± 0.07, n = 10, 6 gerbils, p = 0.605 versus induction, p = 0.005 versus no induction). Thus, iLTP depends on the number of coincident IPSPs and APs, but not their precise relative timing. Additionally, initial experiments showed that iLTP induction was also rate dependent. Similar paired induction protocols at a lower frequency of 100 Hz were only effective at inducing iLTP in low Mg^{2+} artificial cerebral spinal fluid (ACSF, 0.5 mM, Figures S4A–S4C). Together these data suggest a cumulative mechanism based on consistent co-activation.

The involvement of NMDARs was also indicated by Mg^{2+} dependence and the plasticity was blocked by the NMDAR antagonist AP-V (Figures S4A and S4C). Switching to bath application of the use-dependent NMDAR antagonist MK-801 (30 μM), which does not allosterically modulate glycine receptors (GlyRs) as AP-V does (Liu et al., 2010), we found that induction of iLTP in our 200 Hz, standard calcium (1.5 mM) conditions was indeed NMDAR dependent (Figures 3A and 3C: 1.14 ± 0.04, n = 16, 7 gerbils, p = 0.004 versus induction, p = 0.327 versus no induction).

To determine the locus of NMDAR activation, we loaded the recording pipettes with internal solution containing either MK-801 (1 mM) or the calcium chelator BAPTA (15.9 mM) and found that iLTP was disrupted in both cases (Figures 3A–3C: MK-801 pipette, 1.17 ± 0.06, n = 10, 5 gerbils, p = 0.040 versus induction, p = 0.223 versus no induction; BAPTA, 1.01 ± 0.04, n = 8, 3 gerbils, p = 0.004 versus induction, p = 0.337 versus no induction). Consistent with a postsynaptic mechanism, neither the coefficient of variance (CV; Figure 3D: baseline 0.291 ± 0.023, end 0.271 ± 0.023, n = 22, p = 0.213, paired t test) nor the paired-pulse ratio (PPR; Figure 3E: $2^{nd}/1^{st}$, 30 ms interval, baseline 0.985 ± 0.007, end 0.988 ± 0.038, n = 22, p = 0.936, paired t test) of the potentiated IPSPs were altered by iLTP. Together, these data indicate that calcium influx through postsynaptic NMDARs is a critical mechanism underlying iLTP.

In an effort to discover the source of glutamate for NMDAR activation, we investigated the possibility of co-release of glutamate with glycine by MNTB and LNTB neurons as has been observed with MNTB inputs to the lateral superior olive (LSO) (Gillespie et al., 2005; Kim and Kandler, 2010; Noh et al., 2010). To test this possibility, we made whole-cell voltage-clamp recordings from MSO principal neurons, and then used progressively smaller focal applications of glutamate (10 mM) to identify, closely approach, and then electrically stimulate connected inhibitory neurons within either the MNTB or LNTB (Figure 4A, see STAR Methods). The peak amplitudes of the responses were variable and ranged from 146 to 684 pA from the MNTB and 222 to 4,207 pA from the LNTB at –60 mV (Roberts et al., 2014). Once stable responses were recorded at –60 and +35 mV, inhibitory currents were blocked with co-application of glycinergic and

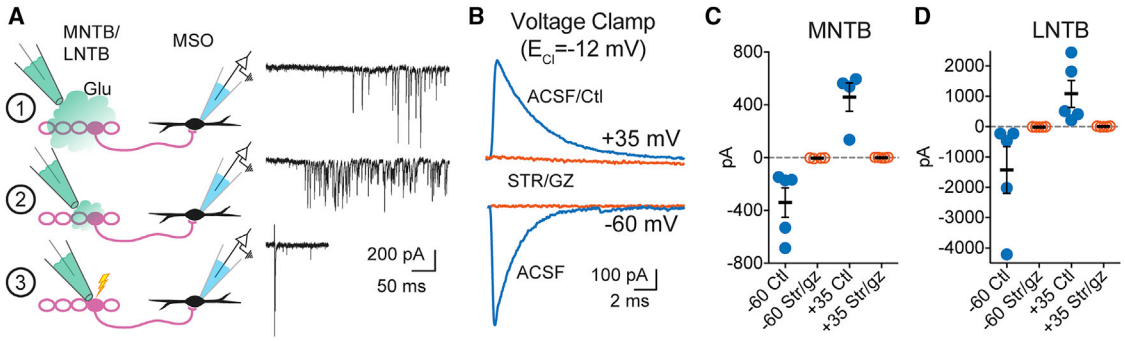

Figure 4. Inhibitory Inputs to the MSO Do Not Co-release Glutamate

(A) Diagram showing the experimental progression of isolating inputs from an LNTB neuron to an MSO neuron using decreasing glutamate puff sizes then switching to electrical stimulation using a combined puff/stimtrode.

(B) Example traces showing synaptic responses in an MSO neuron from the MNTB with the MSO neuron held at +35 mV (top) and –60 mV (bottom) before (blue) and after (orange) blocking inhibition with gabazine (5 μM) and strychnine (1 μM) in the bath.

(C and D) Analysis of responses from MNTB (C) and LNTB (D) stimulation for the peak PSC at different voltages before and after blocking inhibition demonstrating the lack of glutamate-mediated currents from these inputs. Animal ages P12–P15 (13.5 average). Error ± SEM.

$GABA_A$-ergic inhibitory synaptic blockers (Figure 4B; 1 μM strychnine and 5 μM gabazine, respectively; STR and GZ). This would often reveal an unblocked excitatory fiber of passage (~65% of trials) with a fast AMPA mediated current and these trials were discarded. Trials in which all fast transmission were blocked were considered inhibitory-only connections. In these cases, we did not observe any remaining slower NMDAR-mediated currents when stepped to +35 mV to relieve the NMDAR Mg^{2+} block (Figures 4B–4D). In some cases, the stimulation amplitude was subsequently increased to deliberately recruit nearby excitatory fibers of passage (data not shown). These responses exhibited clear AMPA and NMDA components (peak amplitude at –60 mV; –682.44 ± 178.19 pA; at +35 mV, 578.28 ± 208.75 pA, n = 4 each), demonstrating that NMDAR currents would have been detected using our methods, were they present.

Developmental Time Course of Intrinsic Properties and iLTP

iLTP required both AP generation and NMDAR activation. This indicates that APs are sufficiently large to relieve the Mg^{2+} block on NMDARs. However, there is a rapid developmental decrease in spike amplitude and dendritic backpropagation of APs in MSO neurons in the 2 weeks following hearing onset (Scott et al., 2005, 2007). Therefore, we measured BPAPs in MSO neurons just before hearing onset to gauge the full extent of the changes in active and passive membrane properties that occur with hearing. To do this, we made paired dendritic and somatic current-clamp recording from MSO neurons at P9–P11 (P10 average), measured the absolute and relative amplitude of BPAPs and compared these measurements to data obtained at P16–P19 (Figure 5A). Before hearing onset, APs had peak voltages at the soma that were relatively large and narrow (Figures 5A–5C: amplitude, 15.13 ± 1.77 mV, n = 11, 8 gerbils; half-width, 0.39 ± 0.03 ms), and backpropagated effectively into the dendrites with a length constant (λ) of 200 μm (Figure 5D). Just a week later (P16–P19), however, APs exhibit greatly reduced peak voltages (Figures 5A–5C: –19.41 ± 3.06 mV, n = 20, 18 gerbils, $p < 0.0001$), brief duration (0.24 ± 0.01 ms half-width, n = 15, $p < 0.0001$), and are heavily attenuated upon backpropagation into the dendrites (Figures 5B and 5D, λ = 77 μm). These data indicate that the amount of depolarization provided by APs in MSO neurons at the soma and especially in the dendrites decreases dramatically after hearing onset.

In light of these findings, we hypothesized that iLTP may be developmentally limited by the reduced ability of APs to relieve the Mg^{2+} block on NMDARs. To test this, we performed iLTP induction in gerbils at age P18–P20 (P19 average) and found that iLTP was reduced by more than 50% (Figures 6A and 6B: 1.21 ± 0.10, n = 11, 6 gerbils, $p = 0.086$ versus induction, $p = 0.322$ versus no induction). Moreover, in older gerbils (P27–P32, P30 average), we found that iLTP was completely eliminated (Figures 6A and 6B: 0.99 ± 0.07, n = 10, 7 gerbils, $p = 0.002$ versus induction, $p = 0.401$ versus no induction). When we examined the magnitude of iLTP relative to the peak amplitude of the APs in the induction trains, which would differ from rheobase amplitudes for all ages tested (Figure 6C), we found that the younger animals were clustered at the largest AP amplitudes and more consistently showed iLTP. With the intermediate and older ages, there was a range of AP amplitudes, those with larger ones tending to exhibit iLTP. However, the points were scattered and there were not enough of them to correlate the two parameters well.

In order to determine whether the depolarization provided by the AP is a critical element for the developmental time course of iLTP, we made whole-cell recordings from ~P30 MSO neurons with K-gluconate-based internal solutions and paired trains of inhibitory input stimulation with the AP substituted with larger depolarization imposed by voltage-clamp commands (Figure 7A; 2.5 ms voltage-clamp steps to 0 mV). Because of the large voltage-gated currents and necessity of omitting channel blockers, voltage clamp was imperfect at these ages. However, using dual somatic current-clamp/voltage-clamp recordings, we found that 2.5 ms voltage commands from –60 to 0 mV nevertheless substantially increased both the peak amplitude

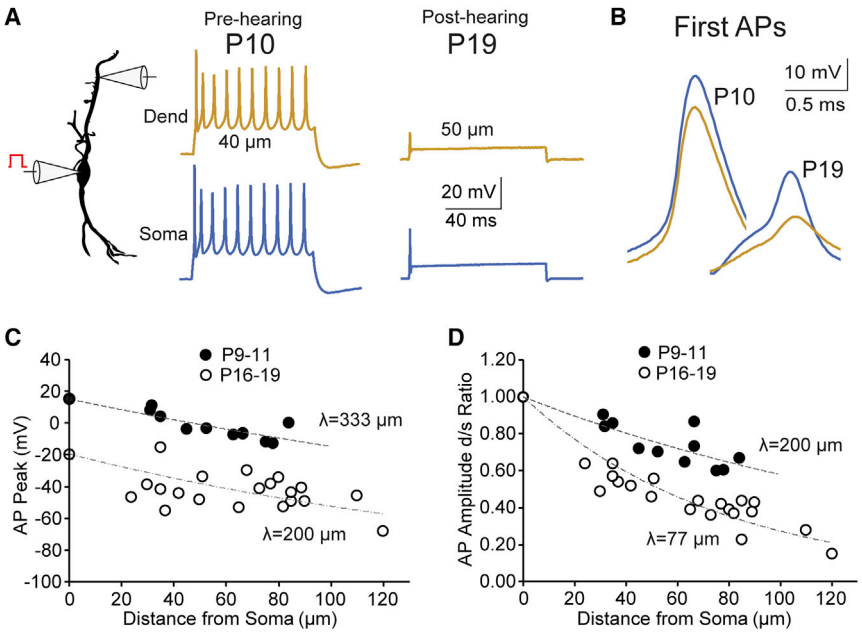

Figure 5. Over the First Week of Hearing, MSO Action Potential Amplitudes and Back-propagation Dramatically Decrease

(A) Simultaneously recorded single traces of dendritic (top) and somatic (bottom) action potentials (APs) elicited by 100 ms current injections into the soma in slices from P10 (left) and P19 (right) gerbils.

(B) Superimposed 1st APs show large amplitude attenuation from soma to dendrite at P19, but not at P10.

(C) AP peak voltage relative to the distance to the dendritic recording location.

(D) Ratio of the AP amplitude from threshold in the dendrite to the soma relative to the distance to the dendritic recording location. Experiments in P16–P19 animals were data reanalyzed from Mathews et al. (2010).

(–16.89 ± 2.66 mV versus –33.96 ± 3.81 mV, n = 4, p = 0.010, paired t test, P29 average) and duration (~2.5 ms versus AP half-width 0.21 ± 0.02 ms, n = 4) of the depolarization beyond natural APs (Figures 7A and 7B). In separate recordings with a single electrode, we delivered iLTP protocols in slices from gerbils P28–P32 (P29.5 average), as in Figure 1A, but replaced the APs with larger depolarizations induced with voltage steps nominally to 0 mV (Figure 7C). This manipulation restored iLTP in older animals (Figures 7D and 7F: V-clamp induction, 1.57 ± 0.14, n = 11, 6 gerbils; voltage step only, 1.10 ± 0.08, n = 8, 3 gerbils, p = 0.017 versus no stim, p = 0.453 versus P12–P15 induction) but was blocked by bath application of MK-801 (30 µM, Figures 7E and 7F: 1.07 ± 0.06, n = 10, 6 gerbils, p = 0.004 versus V-clamp induction). These data suggest that the potential for iLTP is still present in MSO neurons from older animals, but induction is limited by the developmental reduction in the ability of the AP to depolarize the soma and dendrites.

Developmental changes in NMDAR properties might also impact iLTP in older animals. We compared pharmacologically isolated NMDAR synaptic currents from P12–P15 gerbil tissue to those from P29–P33 at holding potentials from −80 to 50 mV (Figures 8A and 8B). In 1 mM Mg^{2+} at +50 mV, responses from older animals were ~3-fold smaller (P12–P15, 391.68 ± 105.69, n = 9, 4 gerbils; P29–P33, 123.26 ± 17.56 mV, n = 8, 3 gerbils, p = 0.032) and there was a trend toward faster initial decays (Figure 8D: tau1 p = 0.064, tau2 p = 0.249) that did not reach significance. We found that at 1 mM Mg^{2+}, the V50 of the conductance normalized to individual Boltzmann fit maximums (Figure 8B insets, see STAR Methods) was shifted toward more depolarized potentials with age (Figure 8C: 5.61 mV, P12–P15, −32.23 ± 0.53 mV, n = 9, 4 gerbils; P29–P33, −26.62 ± 0.99 mV, n = 8, 3 gerbils; p < 0.0001, F = 26.08[1,21], extra sum-of-squares F test) but with very similar slopes (P12–P15, 12.06 ± 0.49; P29–P33, 12.01 ± 0.96; p = 0.968, F = 0.002 [1,21]). However, the reversal potential was higher in the older group (5.19 ± 0.91 mV versus 0.90 ± 0.57 mV, p = 0.001, linear fit from −10 to 20 mV). Steady-state currents at +50 mV were ~2.5 times larger in older animals (P12–P15, 1140.5 ± 76.5 pA, n = 5; P29–P33, 2623.0 ± 300.8 pA, n = 4, p = 0.001), leading to larger voltage errors. A simple voltage error correction using the uncompensated portion of the series resistance (15%) times the voltage command brought the reversal potentials closer (data not shown, 2.57 ± 0.66 mV versus 0.64 ± 0.50 mV, p = 0.032) and yielded Boltzmann fits with similar V50 (P12–P15, −31.68 ± 0.76 mV; P29–P33, −26.42 ± 0.67 mV; p < 0.0001, F = 26.35[1,213], extra sum-of-squares F test) and slope values (P12–P15, 12.46 ± 0.71; P29–P33, 11.79 ± 0.64; p = 511, F = 0.433[1,213]). We also collected NMDAR currents at nominally zero Mg^{2+} and 0.1 mM Mg^{2+}. This slight increase in Mg^{2+} had a clearer effect in the older age group at more depolarized potentials and the variability was larger in the younger group, but the magnitude of the effect was similar at more hyperpolarized potentials (Figures 8E and 8F). We also found that the GluN2B subunit-specific NMDAR antagonist Ro 25-6981 (1 µM) similarly affected synaptic currents in both age groups (Figures 8G and 8H: P12–P13, 43.10% ± 6.52% block, n = 10, 5 gerbils; P30–P31, 47.54% ± 9.15% block, n = 9, 3 gerbils; p = 0.693), suggesting that relative levels of this subunit are stable over the age range iLTP was examined.

DISCUSSION

Neurons in the MSO, like many neurons in both auditory and non-auditory subcortical pathways, encode information at rates of up to hundreds of hertz. The high frequency of firing may preclude these neurons from using conventional spike-timing-dependent learning rules, which rely on relatively slow intracellular biochemical pathways to unambiguously report the phase relationship between synaptic input and spiking activity. Here we show at inhibitory synapses onto MSO neurons that, indeed, iLTP is insensitive to within-cycle phase relationships between IPSPs and APs. Instead, we describe a form of plasticity that requires

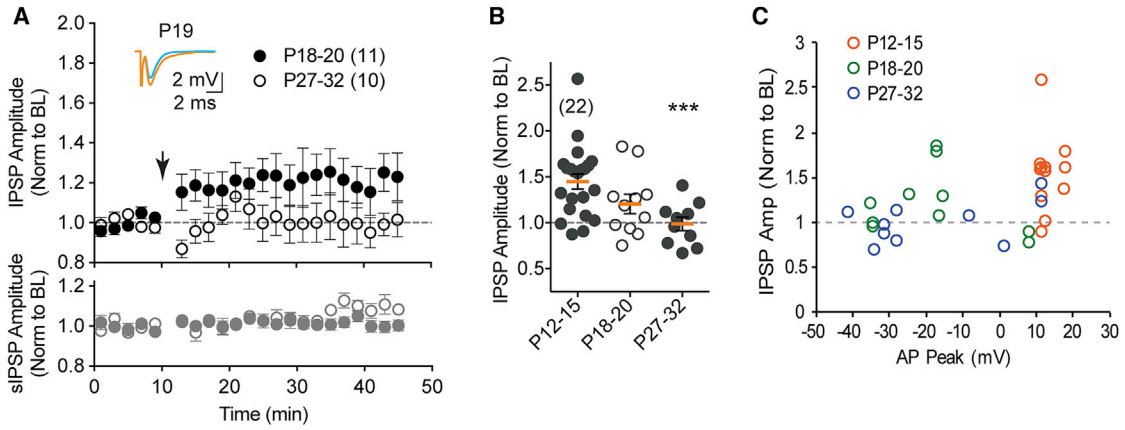

Figure 6. iLTP Induction Is Progressively Eliminated over the First 2 Weeks of Hearing

(A) Group data showing lack of iLTP in young adult gerbils (open) and intermediate iLTP at an intermediate age (filled).

(B) Average of the last 10 min of the group data for each age with the P12–P15 group from 1F for comparison.

(C) The average of the last 10 min for each cell grouped by age and plotted relative to the peak voltage of the AP in the induction train. Error ± SEM. ***$p \leq 0.001$.

the integration of coactive IPSPs and APs at higher frequencies where the range of possible intervals is approximately an order of magnitude shorter than those typically observed in STDP experiments. This form of iLTP involves calcium influx triggered through the cooperative action of APs and NMDARs. We further show that a developmental reduction in the amplitude and dendritic backpropagation of APs in MSO neurons dictates a window for iLTP induction on these neurons lasting ~2 weeks after hearing onset. These results reveal an intricate coordination between the developmental regulation of voltage-gated ion channels and adjustments in the strength of inhibition.

iLTP Induction Protocol and Timing

While investigations into the mechanisms of synaptic plasticity are driven by the need to understand associative learning, such studies have also been used to reveal the rules regulating the development of brain circuits. It has become clear that inhibition must coincide in time with excitation to effectively influence neuronal computations and some cellular mechanisms that would link them have been elucidated (D'amour and Froemke, 2015; Okun and Lampl, 2008; Wehr and Zador, 2003). However, inhibitory synaptic plasticity has mostly been explored in systems that employ sparse firing network dynamics (Vogels et al., 2011), where synaptic potentiation or depression is determined by the now-standard STDP paradigms in which pairing of a few or even single presynaptic/postsynaptic activations with relative timings in the tens of milliseconds (Vogels et al., 2013). Indeed, STDP rules in the auditory system can operate over shorter time windows (Tzounopoulos et al., 2004).

An STDP mechanism with a learning window that extends over milliseconds has been proposed as a mechanism to instruct the formation of appropriate excitatory delay lines in the avian equivalent of the MSO circuit (Gerstner et al., 1996), but this concept has never been tested experimentally. Our present experiments, which test inhibitory and not excitatory plasticity, argue that synaptic plasticity is not dependent on fine-scale synaptic timing along the lines of an STDP mechanism. iLTP builds slowly and cumulatively over many stimulus repetitions, a finding that may be more consonant with the higher (>100 Hz) rates of synaptic and AP firing activity in the MSO as compared with most neurons (Dehmel et al., 2010; Franken et al., 2015; Joris et al., 1994; Kuenzel et al., 2011; van der Heijden et al., 2013). At 200 Hz, the frequency of stimulation in most of our experiments, the 2.5 ms time window, accounting for phase ambiguity in trains, is likely too narrow in comparison to the duration of intracellular calcium transients for the neuron to distinguish fine relative timing information. A caveat in these slice experiments is that inhibitory and excitatory inputs are necessarily synchronously co-activated, and thus may not accurately reflect physiological differences in relative timing that arise from differences in tonotopic position and other factors. However, the insensitivity of iLTP to the timing between synaptic stimuli and APs argues that such excitatory/inhibitory timing differences may not be important determinants of synapse reinforcement.

In comparison to an STDP mechanism, where relatively fewer pre-post pairings occurring over a time window of tens of milliseconds drives large changes in synaptic strength, a more cumulative induction process may be a more stable way to establish an appropriate balance between excitation and inhibition. This cumulative hypothesis is also consistent with our findings that iLTP was sensitive to decreasing the rate (Figure S4) or number (Figures 2D and 2E) of pre-post pairings. However, since AMPARs, some of which may be calcium permeable (Smith et al., 2000), were necessarily blocked to visualize IPSPs, the sensitivity of iLTP to these stimuli could be underestimated.

iLTP Mechanism and Cell Signaling Pathways

Developmental plasticity at inhibitory synapses has been intensively studied when the concentration of intracellular chloride is high, thus allowing inhibitory synapses to provide their own excitation (Ben-Ari, 2002; Noh et al., 2010). However, in the MSO and many other brain regions, changes to inhibitory inputs occur well after the developmental expression of chloride-potassium co-transporters hyperpolarizes the chloride equilibrium

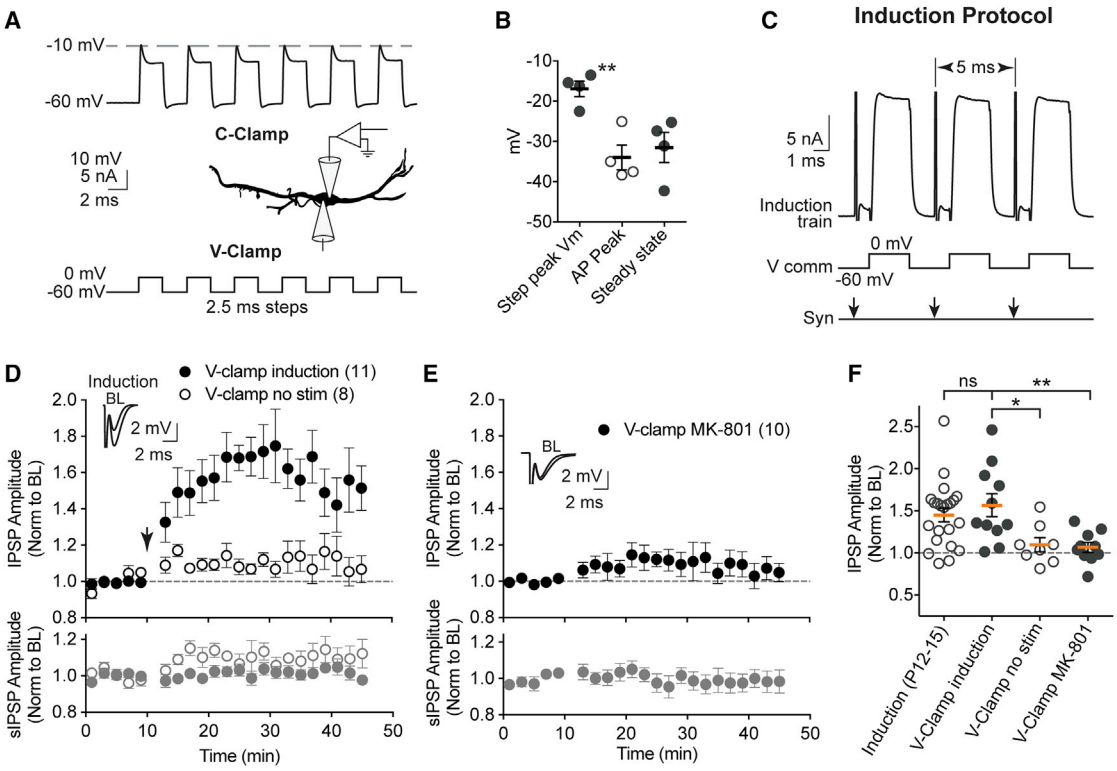

Figure 7. iLTP in Young Adult Animals Is Rescued by Larger Depolarizations

(A) Traces from a dual soma patched cell showing a small part of a train of voltage-clamp steps from –60 to 0 mV (bottom) and resultant current-clamp responses (top) in a cell from P29 tissue.

(B) Summary data from dual somatic voltage-clamp/current-clamp train recordings (n = 4, P29 average) showing the average peak voltage during the step, steady state during the step, and the endogenous AP peak. AP peak is compared to step peak.

(C) Diagram showing a small portion of the voltage-clamp trace (top) during the AP replacement induction protocol with voltage steps (V comm) and electrical stimulation of inputs (Syn).

(D) Group data showing iLTP with the paired voltage-clamp protocol and no iLTP from voltage steps alone. P28–P32, P29.5 average.

(E) Group data showing block of iLTP with the voltage-clamp protocol by the NMDAR antagonist MK-801 (30 μM).

(F) Average of the last 10 min of the group data for voltage-clamp protocols with the P12–P15 group from Figure 1F for comparison. Error ± SEM. *$p \leq 0.05$, **$p \leq 0.01$.

potential below firing threshold (Ben-Ari et al., 1989; Löhrke et al., 2005; Milenković and Rübsamen, 2011; Obata et al., 1978). The work presented here suggests that in the MSO, self-depolarization is replaced by cooperativity between BPAPs and synaptic activation through NMDARs (Figure 1). This would selectively preserve and strengthen inhibitory inputs co-active with strong binaural excitatory drive.

Our data support a model in which postsynaptic calcium entry via NMDARs initiates iLTP (Figure 3). While we cannot rule out additional sources of calcium, our data are consistent with known calcium-mediated signaling systems that can potentiate glycinergic synapses. In spinal nerve cell cultures, a similar signaling cascade involving synaptic activity, calcium entry, and NMDAR activation has been shown to initiate glycine receptor (GlyR) synaptic clustering (Lévi et al., 2008). In this culture system, GlyRs are strongly depolarizing and GlyR activity is required for clustering (Lévi et al., 1998). Additionally, *in vivo* GlyR clustering in zebrafish larva depend on calcium-calmodulin-dependent protein kinase II (CamKII) and L-type calcium channels (Oda et al., 1995; Yamanaka et al., 2013). The scaffolding protein gephyrin is required for GlyR capture at synapses and has been implicated in changes in synaptic strength via phosphorylation cascades involving CamKII, which is often scaffolded downstream of NMDARs, as well as integrin cell adhesion molecules (Calamai et al., 2009; Charrier et al., 2010; Dumoulin et al., 2010; Kirsch et al., 1993). It has also been observed that increasing excitatory drive onto spinal interneurons increases GlyR clustering (Gonzalez-Forero et al., 2005) and interleukin1 beta via calcium influx can potentiate GlyR responses (Chirila et al., 2014).

Our findings would also be consistent with post-translational modification of GlyRs receptors that modulate the single-channel conductance or open probability that may also be activated by calcium influx via protein kinase C, CamKII, or endocannabinoids (Albarran et al., 2001; Fucile et al., 2000; Lozovaya et al., 2011; Ren et al., 1998; Song and Huang, 1990; Wang and Randić, 1996).

Mechanisms in which synaptic potentiation maintains connections have also been hypothesized to refine inhibitory inputs onto neurons of the lateral superior olive (LSO), which also receives glycinergic inhibition from the MNTB, largely prior to hearing

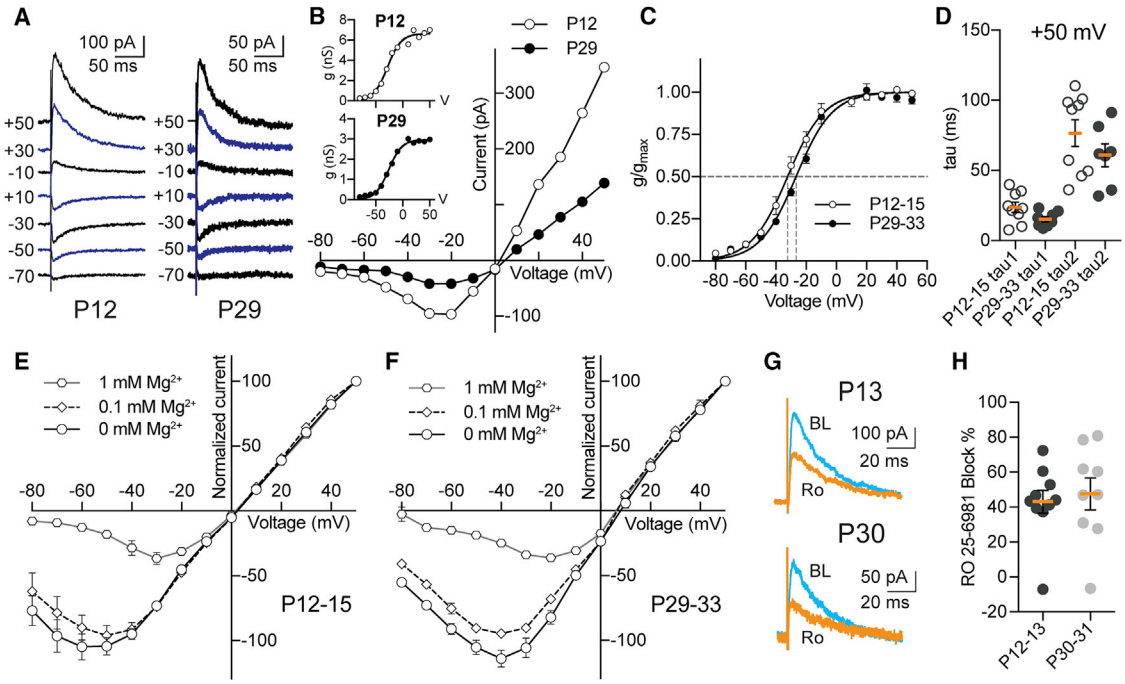

Figure 8. Synaptic NMDARs Exhibit Similarities but Greater Voltage Dependence with Age

(A) Averaged and AP-V (50 μM) subtracted example traces from P12 and P29 tissue at the voltage steps shown in 1 mM Mg^{2+}.

(B) Voltage/current relationships for the two cells shown in (A), insets are conductances fit with Boltzmann equations used to calculate g_{max}.

(C) Normalized conductance group data fit with Boltzmann equations, dashed lines showing V50.

(D) Group data for decay constants of the +50 mV average traces.

(E and F) Group data for young (E) and old (F) animals for the three levels of Mg^{2+} shown.

(G) Average example traces from P13 and P30 tissue showing the effects of GluN2B subunit block by Ro 25-6981 (1 μM); BL, baseline.

(H) Group data for GluN2B subunit block. Error ± SEM.

onset when these inputs are depolarizing and excitatory (Chang et al., 2003; Noh et al., 2010). It has also been reported that LTP at glycinergic synapses could be induced in the LSO shortly after hearing onset (Kotak and Sanes, 2014). These authors found that $GABA_B$ receptor activation was required for LTP in response to long depolarizations (~1 hr at 0 mV) of the postsynaptic cell and stimulation of MNTB afferents with ionotropic glutamate receptors blocked. We did not find that $GABA_B$ receptor block affected iLTP in the MSO, although our experimental conditions are quite different (Figure S4). In addition, these authors found that relatively shorter depolarizations (0.5 s) also implicated glutamatergic signaling in the induction of inhibitory plasticity with bath application of glutamate. In the LSO, the question remains how inhibitory input strength is appropriately adjusted under physiological conditions, where after hearing onset synaptic excitation is brief, and both synaptic and firing rates extend to hundreds of hertz. The learning rule underlying the plasticity we have identified here, where inhibitory strength is adjusted cumulatively in smaller increments, integrating the activity of co-activated glycinergic and glutamatergic inputs over longer (e.g., minutes) periods, may well apply to the LSO. Further, our work shows that iLTP is exhibited over a limited time window that is defined by developmental changes in passive and active intrinsic properties in the cell. It will be important to assess how the development of intrinsic properties shapes iLTP in the LSO and other brainstem auditory neurons that utilize temporal codes.

It remains to be determined whether the NMDARs underlying iLTP are located directly at the potentiated glycinergic synapses or heterosynaptic plasticity drives iLTP through adjacent excitatory synapses. Well before hearing onset, NMDARs are present at synapses between MNTB and LSO neurons and help drive synapse formation (Gillespie et al., 2005; Kim and Kandler, 2010). Thus, it is possible that glycinergic synapses still harbor NMDARs after hearing onset. Related to this question is how synapse specificity might be enforced. Glycine released from activated inhibitory synapses would occupy the obligatory glycine binding site on NMDARs, perhaps spatially limiting NMDAR activation to activated inhibitory inputs.

We did not find evidence for co-release of glutamate and glycine from MNTB or LNTB terminals in the MSO (Figure 4), as has been shown to occur at MNTB-LSO synapses (Gillespie et al., 2005; Noh et al., 2010). If NMDARs involved in iLTP are located at inhibitory synapses in the MSO, glutamate for NMDAR activation may come from spillover from excitatory terminals that are intermingled and evenly distributed with inhibitory terminals at the soma and proximal dendrites (Clark, 1969; Russell and Moore, 2002; Tirko and Ryugo, 2012). It has been noted that in the MSO of gerbils, some parts of afferent terminals containing clathrin-coated pits are located

very near, but not directly on, target dendrites (Russell and Moore, 2002). Such terminals have been proposed to underlie sustained transmitter release (Brodin et al., 1997). It has also been suggested that in the MSO of gerbils, the inhibitory and excitatory synapses are in close enough proximity for spillover of glycine in the opposite direction to potentiate NMDAR responses at excitatory synapses (Couchman et al., 2012). Reliance on spillover would potentially widen the window of coincidental activation for inhibition.

Developmental Time Course of MSO Intrinsic Properties and iLTP

Over the first 2 weeks of hearing, MSO principal neurons undergo developmental changes in both ligand- and voltage-gated ion channels that electrically isolates the AP from the soma and dendrites and reduces the time course of synaptic integration from tens of milliseconds to a few hundred microseconds (Chirila et al., 2007; Khurana et al., 2012; Magnusson et al., 2005; Mathews et al., 2010; Myoga et al., 2014; Scott et al., 2005). We found that these physiological changes limit the induction of iLTP (Figure 6) and stabilize the magnitude of synaptic inhibition. However, we could rescue iLTP at older ages (Figure 7), suggesting that the cellular mechanisms for iLTP induction remain operational, possibly playing a subtler role in maintaining synaptic inputs. Maintaining the capacity for plasticity into maturity may be important for facilitating recovery from sensory perturbations. Consistent with this idea, the strength of aberrant inhibitory inputs in the MSO of congenitally deaf cats have been found to be normalized following cochlear implantation (Tirko and Ryugo, 2012). In addition, interference with normal binaural auditory experience in gerbils via rearing in omnidirectional noise produce only temporary disruptions in inhibitory input development and sound localization performance (Kapfer et al., 2002; Maier et al., 2008).

Since it is necessary to block AMPARs to measure GlyR responses, we cannot assess how having simultaneous activation of AMPARs would affect iLTP induction at older ages. It is possible that iLTP is underestimated in our experiments. AMPARs in mature MSO neurons likely exhibit high calcium permeability (Parks, 2000; Sato et al., 2000) and this additional source of calcium could potentially contribute to iLTP. Having local AMPA-mediated depolarization intact could extend the ages when iLTP can be induced. However, in more mature MSO neurons (>P28), NMDAR responses are not observed with synaptic stimulation from resting membrane potential at 35°C. This may reflect the kinetics of NMDAR Mg^{2+} dependence relative to the very brief AMPAR currents (Kampa et al., 2004; Vargas-Caballero and Robinson, 2003) or the increasing segregation of synaptic NMDARs to the dendrites.

We found that the voltage dependence of synaptic NMDARs increased only modestly with age (Figure 8C). This observation along with the NMDAR decay time constants we observed are not consistent with the large increases in GluN2C expression observed with age in the LSO (Pilati et al., 2016) and MNTB (Steinert et al., 2010). There also does not appear to be a shift in synaptic GluN2B expression after hearing onset in the MSO (Figure 8H) as is the case in many other brain regions (Cull-Candy et al., 2001; Sanchez et al., 2015). However, this observation is consistent with reports that MSO neurons express GluN2A/B receptor subunits throughout development (Caicedo and Eybalin, 1999; Sato et al., 1999). Further studies are needed to fully assess developmental NMDAR subunit expression in the MSO, but these data suggest relative consistency over the age range we observed iLTP.

Changes in synaptic strength have been shown to be an important determinant of the subsequent physical restructuring and maintenance of synaptic connections in multiple brain areas (Andreae and Burrone, 2014; Kwon and Sabatini, 2011; Nishiyama, 2014; Sorra and Harris, 1998; Yuste and Bonhoeffer, 2001). We found that after hearing onset the developing intrinsic properties of MSO, neurons drive down AP amplitudes and decrease AP backpropagation into the dendrites (Figure 5). We also showed that iLTP critically depends on the amount of AP depolarization in older animals (Figure 7). Thus, the developing intrinsic properties would progressively reduce reinforcement of more distal inhibitory synapses, potentially leading to their weakening and eventual removal. Such a mechanism may contribute to the activity-dependent redistribution of dendritic inhibitory synapses toward the soma and proximal dendrites that have been observed (Kapfer et al., 2002; Werthat et al., 2008).

STAR★METHODS

Detailed methods are provided in the online version of this paper and include the following:

- KEY RESOURCES TABLE
- CONTACT FOR REAGENT AND RESOURCE SHARING
- EXPERIMENTAL MODEL AND SUBJECT DETAILS
- METHOD DETAILS
  - Tissue preparation
  - Electrophysiology
- QUANTIFICATION AND STATISTICAL ANALYSIS

SUPPLEMENTAL INFORMATION

Supplemental Information includes four figures and can be found with this article online at https://doi.org/10.1016/j.neuron.2018.03.001.

ACKNOWLEDGMENTS

This work was supported by the United States National Institutes of Health (RO1 DC006877 to N.L.G. and F32 DC014890 to B.D.W.).

AUTHOR CONTRIBUTIONS

B.D.W and N.L.G. conducted experiments, designed research, and wrote the manuscript.

DECLARATION OF INTERESTS

The authors declare no competing interests.

Received: June 27, 2017
Revised: January 9, 2018
Accepted: February 28, 2018
Published: March 22, 2018

REFERENCES

Albarran, F.A., Roa, J.P., Navarrete, R., Castillo, R., Nualart, F., and Aguayo, L.G. (2001). Effect of protein kinase C activation on the glycine evoked Cl(-) current in spinal cord neurons. Brain Res. *902*, 1–10.

Andreae, L.C., and Burrone, J. (2014). The role of neuronal activity and transmitter release on synapse formation. Curr. Opin. Neurobiol. *27*, 47–52.

Ben-Ari, Y. (2002). Excitatory actions of gaba during development: the nature of the nurture. Nat. Rev. Neurosci. *3*, 728–739.

Ben-Ari, Y., Cherubini, E., Corradetti, R., and Gaiarsa, J.L. (1989). Giant synaptic potentials in immature rat CA3 hippocampal neurones. J. Physiol. *416*, 303–325.

Brand, A., Behrend, O., Marquardt, T., McAlpine, D., and Grothe, B. (2002). Precise inhibition is essential for microsecond interaural time difference coding. Nature *417*, 543–547.

Brodin, L., Löw, P., Gad, H., Gustafsson, J., Pieribone, V.A., and Shupliakov, O. (1997). Sustained neurotransmitter release: new molecular clues. Eur. J. Neurosci. *9*, 2503–2511.

Caicedo, A., and Eybalin, M. (1999). Glutamate receptor phenotypes in the auditory brainstem and mid-brain of the developing rat. Eur. J. Neurosci. *11*, 51–74.

Calamai, M., Specht, C.G., Heller, J., Alcor, D., Machado, P., Vannier, C., and Triller, A. (2009). Gephyrin oligomerization controls GlyR mobility and synaptic clustering. J. Neurosci. *29*, 7639–7648.

Cant, N.B., and Hyson, R.L. (1992). Projections from the lateral nucleus of the trapezoid body to the medial superior olivary nucleus in the gerbil. Hear. Res. *58*, 26–34.

Chang, E.H., Kotak, V.C., and Sanes, D.H. (2003). Long-term depression of synaptic inhibition is expressed postsynaptically in the developing auditory system. J. Neurophysiol. *90*, 1479–1488.

Charrier, C., Machado, P., Tweedie-Cullen, R.Y., Rutishauser, D., Mansuy, I.M., and Triller, A. (2010). A crosstalk between β1 and β3 integrins controls glycine receptor and gephyrin trafficking at synapses. Nat. Neurosci. *13*, 1388–1395.

Chirila, F.V., Rowland, K.C., Thompson, J.M., and Spirou, G.A. (2007). Development of gerbil medial superior olive: integration of temporally delayed excitation and inhibition at physiological temperature. J. Physiol. *584*, 167–190.

Chirila, A.M., Brown, T.E., Bishop, R.A., Bellono, N.W., Pucci, F.G., and Kauer, J.A. (2014). Long-term potentiation of glycinergic synapses triggered by interleukin 1β. Proc. Natl. Acad. Sci. USA *111*, 8263–8268.

Clark, G.M. (1969). The ultrastructure of nerve endings in the medial superior olive of the cat. Brain Res. *14*, 293–305.

Couchman, K., Grothe, B., and Felmy, F. (2010). Medial superior olivary neurons receive surprisingly few excitatory and inhibitory inputs with balanced strength and short-term dynamics. J. Neurosci. *30*, 17111–17121.

Couchman, K., Grothe, B., and Felmy, F. (2012). Functional localization of neurotransmitter receptors and synaptic inputs to mature neurons of the medial superior olive. J. Neurophysiol. *107*, 1186–1198.

Cull-Candy, S., Brickley, S., and Farrant, M. (2001). NMDA receptor subunits: diversity, development and disease. Curr. Opin. Neurobiol. *11*, 327–335.

D'amour, J.A., and Froemke, R.C. (2015). Inhibitory and excitatory spike-timing-dependent plasticity in the auditory cortex. Neuron *86*, 514–528.

Dehmel, S., Kopp-Scheinpflug, C., Weick, M., Dörrscheidt, G.J., and Rübsamen, R. (2010). Transmission of phase-coupling accuracy from the auditory nerve to spherical bushy cells in the Mongolian gerbil. Hear. Res. *268*, 234–249.

Dumoulin, A., Triller, A., and Kneussel, M. (2010). Cellular transport and membrane dynamics of the glycine receptor. Front. Mol. Neurosci. *2*, 28.

Feldman, D.E. (2012). The spike-timing dependence of plasticity. Neuron *75*, 556–571.

Franken, T.P., Roberts, M.T., Wei, L., Golding, N.L., and Joris, P.X. (2015). In vivo coincidence detection in mammalian sound localization generates phase delays. Nat. Neurosci. *18*, 444–452.

Fucile, S., De Saint Jan, D., de Carvalho, L.P., and Bregestovski, P. (2000). Fast potentiation of glycine receptor channels of intracellular calcium in neurons and transfected cells. Neuron *28*, 571–583.

Gerstner, W., Kempter, R., van Hemmen, J.L., and Wagner, H. (1996). A neuronal learning rule for sub-millisecond temporal coding. Nature *383*, 76–81.

Gillespie, D.C., Kim, G., and Kandler, K. (2005). Inhibitory synapses in the developing auditory system are glutamatergic. Nat. Neurosci. *8*, 332–338.

Goldberg, J.M., and Brown, P.B. (1969). Response of binaural neurons of dog superior olivary complex to dichotic tonal stimuli: some physiological mechanisms of sound localization. J. Neurophysiol. *32*, 613–636.

Gonzalez-Forero, D., Pastor, A.M., Geiman, E.J., Benítez-Temiño, B., and Alvarez, F.J. (2005). Regulation of gephyrin cluster size and inhibitory synaptic currents on Renshaw cells by motor axon excitatory inputs. J. Neurosci. *25*, 417–429.

Grothe, B., and Sanes, D.H. (1993). Bilateral inhibition by glycinergic afferents in the medial superior olive. J. Neurophysiol. *69*, 1192–1196.

Grothe, B., and Sanes, D.H. (1994). Synaptic inhibition influences the temporal coding properties of medial superior olivary neurons: an in vitro study. J. Neurosci. *14*, 1701–1709.

Joris, P.X., Carney, L.H., Smith, P.H., and Yin, T.C. (1994). Enhancement of neural synchronization in the anteroventral cochlear nucleus. I. Responses to tones at the characteristic frequency. J. Neurophysiol. *71*, 1022–1036.

Kampa, B.M., Clements, J., Jonas, P., and Stuart, G.J. (2004). Kinetics of Mg2+ unblock of NMDA receptors: implications for spike-timing dependent synaptic plasticity. J. Physiol. *556*, 337–345.

Kapfer, C., Seidl, A.H., Schweizer, H., and Grothe, B. (2002). Experience-dependent refinement of inhibitory inputs to auditory coincidence-detector neurons. Nat. Neurosci. *5*, 247–253.

Khurana, S., Liu, Z., Lewis, A.S., Rosa, K., Chetkovich, D., and Golding, N.L. (2012). An essential role for modulation of hyperpolarization-activated current in the development of binaural temporal precision. J. Neurosci. *32*, 2814–2823.

Kim, G., and Kandler, K. (2010). Synaptic changes underlying the strengthening of GABA/glycinergic connections in the developing lateral superior olive. Neuroscience *171*, 924–933.

Kirsch, J., Wolters, I., Triller, A., and Betz, H. (1993). Gephyrin antisense oligonucleotides prevent glycine receptor clustering in spinal neurons. Nature *366*, 745–748.

Kotak, V.C., and Sanes, D.H. (2014). Developmental expression of inhibitory synaptic long-term potentiation in the lateral superior olive. Front. Neural Circuits *8*, 67.

Kuenzel, T., Borst, J.G., and van der Heijden, M. (2011). Factors controlling the input-output relationship of spherical bushy cells in the gerbil cochlear nucleus. J. Neurosci. *31*, 4260–4273.

Kwon, H.B., and Sabatini, B.L. (2011). Glutamate induces de novo growth of functional spines in developing cortex. Nature *474*, 100–104.

Lévi, S., Vannier, C., and Triller, A. (1998). Strychnine-sensitive stabilization of postsynaptic glycine receptor clusters. J. Cell Sci. *111*, 335–345.

Lévi, S., Schweizer, C., Bannai, H., Pascual, O., Charrier, C., and Triller, A. (2008). Homeostatic regulation of synaptic GlyR numbers driven by lateral diffusion. Neuron *59*, 261–273.

Liu, J., Wu, D.C., and Wang, Y.T. (2010). Allosteric potentiation of glycine receptor chloride currents by glutamate. Nat. Neurosci. *13*, 1225–1232.

Löhrke, S., Srinivasan, G., Oberhofer, M., Doncheva, E., and Friauf, E. (2005). Shift from depolarizing to hyperpolarizing glycine action occurs at different perinatal ages in superior olivary complex nuclei. Eur. J. Neurosci. *22*, 2708–2722.

Lorteije, J.A., Rusu, S.I., Kushmerick, C., and Borst, J.G. (2009). Reliability and precision of the mouse calyx of Held synapse. J. Neurosci. *29*, 13770–13784.

Lozovaya, N., Mukhtarov, M., Tsintsadze, T., Ledent, C., Burnashev, N., and Bregestovski, P. (2011). Frequency-Dependent Cannabinoid Receptor-Independent Modulation of Glycine Receptors by Endocannabinoid 2-AG. Front. Mol. Neurosci. *4*, 13.

Magnusson, A.K., Kapfer, C., Grothe, B., and Koch, U. (2005). Maturation of glycinergic inhibition in the gerbil medial superior olive after hearing onset. J. Physiol. *568*, 497–512.

Maier, J.K., Kindermann, T., Grothe, B., and Klump, G.M. (2008). Effects of omni-directional noise-exposure during hearing onset and age on auditory spatial resolution in the Mongolian gerbil (Meriones unguiculatus) – a behavioral approach. Brain Res. *1220*, 47–57.

Mathews, P.J., Jercog, P.E., Rinzel, J., Scott, L.L., and Golding, N.L. (2010). Control of submillisecond synaptic timing in binaural coincidence detectors by K(v)1 channels. Nat. Neurosci. *13*, 601–609.

Mc Laughlin, M., van der Heijden, M., and Joris, P.X. (2008). How secure is in vivo synaptic transmission at the calyx of Held? J. Neurosci. *28*, 10206–10219.

McFadden, S.L., Walsh, E.J., and McGee, J. (1996). Onset and development of auditory brainstem responses in the Mongolian gerbil (Meriones unguiculatus). Hear. Res. *100*, 68–79.

Milenković, I., and Rübsamen, R. (2011). Development of the chloride homeostasis in the auditory brainstem. Physiol. Res. *60* (*Suppl 1*), S15–S27.

Myoga, M.H., Lehnert, S., Leibold, C., Felmy, F., and Grothe, B. (2014). Glycinergic inhibition tunes coincidence detection in the auditory brainstem. Nat. Commun. *5*, 3790.

Nishiyama, H. (2014). Learning-induced structural plasticity in the cerebellum. Int. Rev. Neurobiol. *117*, 1–19.

Noh, J., Seal, R.P., Garver, J.A., Edwards, R.H., and Kandler, K. (2010). Glutamate co-release at GABA/glycinergic synapses is crucial for the refinement of an inhibitory map. Nat. Neurosci. *13*, 232–238.

Obata, K., Oide, M., and Tanaka, H. (1978). Excitatory and inhibitory actions of GABA and glycine on embryonic chick spinal neurons in culture. Brain Res. *144*, 179–184.

Oda, Y., Charpier, S., Murayama, Y., Suma, C., and Korn, H. (1995). Long-term potentiation of glycinergic inhibitory synaptic transmission. J. Neurophysiol. *74*, 1056–1074.

Okun, M., and Lampl, I. (2008). Instantaneous correlation of excitation and inhibition during ongoing and sensory-evoked activities. Nat. Neurosci. *11*, 535–537.

Parks, T.N. (2000). The AMPA receptors of auditory neurons. Hear. Res. *147*, 77–91.

Pecka, M., Brand, A., Behrend, O., and Grothe, B. (2008). Interaural time difference processing in the mammalian medial superior olive: the role of glycinergic inhibition. J. Neurosci. *28*, 6914–6925.

Perkins, R.E. (1973). An electron microscopic study of synaptic organization in the medial superior olive of normal and experimental chinchillas. J. Comp. Neurol. *148*, 387–415.

Pilati, N., Linley, D.M., Selvaskandan, H., Uchitel, O., Hennig, M.H., Kopp-Scheinpflug, C., and Forsythe, I.D. (2016). Acoustic trauma slows AMPA receptor-mediated EPSCs in the auditory brainstem, reducing GluA4 subunit expression as a mechanism to rescue binaural function. J. Physiol. *594*, 3683–3703.

Rautenberg, P.L., Grothe, B., and Felmy, F. (2009). Quantification of the three-dimensional morphology of coincidence detector neurons in the medial superior olive of gerbils during late postnatal development. J. Comp. Neurol. *517*, 385–396.

Recio-Spinoso, A. (2012). Enhancement and distortion in the temporal representation of sounds in the ventral cochlear nucleus of chinchillas and cats. PLoS ONE *7*, e44286.

Ren, J., Ye, J.H., and McArdle, J.J. (1998). cAMP-dependent protein kinase modulation of glycine-activated chloride current in neurons freshly isolated from rat ventral tegmental area. Brain Res. *811*, 71–78.

Roberts, M.T., Seeman, S.C., and Golding, N.L. (2013). A mechanistic understanding of the role of feedforward inhibition in the mammalian sound localization circuitry. Neuron *78*, 923–935.

Roberts, M.T., Seeman, S.C., and Golding, N.L. (2014). The relative contributions of MNTB and LNTB neurons to inhibition in the medial superior olive assessed through single and paired recordings. Front. Neural Circuits *8*, 49.

Russell, F.A., and Moore, D.R. (2002). Ultrastructural transynaptic effects of unilateral cochlear ablation in the gerbil medial superior olive. Hear. Res. *173*, 43–61.

Sanchez, J.T., Ghelani, S., and Otto-Meyer, S. (2015). From development to disease: diverse functions of NMDA-type glutamate receptors in the lower auditory pathway. Neuroscience *285*, 248–259.

Sato, K., Nakagawa, H., Kuriyama, H., and Altschuler, R.A. (1999). Differential distribution of N-methyl-D-aspartate receptor-2 subunit messenger RNA in the rat superior olivary complex. Neuroscience *89*, 839–853.

Sato, K., Shiraishi, S., Nakagawa, H., Kuriyama, H., and Altschuler, R.A. (2000). Diversity and plasticity in amino acid receptor subunits in the rat auditory brain stem. Hear. Res. *147*, 137–144.

Scott, L.L., Mathews, P.J., and Golding, N.L. (2005). Posthearing developmental refinement of temporal processing in principal neurons of the medial superior olive. J. Neurosci. *25*, 7887–7895.

Scott, L.L., Hage, T.A., and Golding, N.L. (2007). Weak action potential backpropagation is associated with high-frequency axonal firing capability in principal neurons of the gerbil medial superior olive. J. Physiol. *583*, 647–661.

Sjöström, P.J., Turrigiano, G.G., and Nelson, S.B. (2001). Rate, timing, and cooperativity jointly determine cortical synaptic plasticity. Neuron *32*, 1149–1164.

Smith, P.H., Joris, P.X., Carney, L.H., and Yin, T.C. (1991). Projections of physiologically characterized globular bushy cell axons from the cochlear nucleus of the cat. J. Comp. Neurol. *304*, 387–407.

Smith, A.J., Owens, S., and Forsythe, I.D. (2000). Characterisation of inhibitory and excitatory postsynaptic currents of the rat medial superior olive. J. Physiol. *529*, 681–698.

Song, Y.M., and Huang, L.Y. (1990). Modulation of glycine receptor chloride channels by cAMP-dependent protein kinase in spinal trigeminal neurons. Nature *348*, 242–245.

Sorra, K.E., and Harris, K.M. (1998). Stability in synapse number and size at 2 hr after long-term potentiation in hippocampal area CA1. J. Neurosci. *18*, 658–671.

Spirou, G.A., Brownell, W.E., and Zidanic, M. (1990). Recordings from cat trapezoid body and HRP labeling of globular bushy cell axons. J. Neurophysiol. *63*, 1169–1190.

Spitzer, M.W., and Semple, M.N. (1995). Neurons sensitive to interaural phase disparity in gerbil superior olive: diverse monaural and temporal response properties. J. Neurophysiol. *73*, 1668–1690.

Steinert, J.R., Postlethwaite, M., Jordan, M.D., Chernova, T., Robinson, S.W., and Forsythe, I.D. (2010). NMDAR-mediated EPSCs are maintained and accelerate in time course during maturation of mouse and rat auditory brainstem in vitro. J. Physiol. *588*, 447–463.

Tirko, N.N., and Ryugo, D.K. (2012). Synaptic plasticity in the medial superior olive of hearing, deaf, and cochlear-implanted cats. J. Comp. Neurol. *520*, 2202–2217.

Tzounopoulos, T., Kim, Y., Oertel, D., and Trussell, L.O. (2004). Cell-specific, spike timing-dependent plasticities in the dorsal cochlear nucleus. Nat. Neurosci. *7*, 719–725.

van der Heijden, M., Lorteije, J.A., Plauška, A., Roberts, M.T., Golding, N.L., and Borst, J.G. (2013). Directional hearing by linear summation of binaural inputs at the medial superior olive. Neuron *78*, 936–948.

Vargas-Caballero, M., and Robinson, H.P. (2003). A slow fraction of Mg2+ unblock of NMDA receptors limits their contribution to spike generation in cortical pyramidal neurons. J. Neurophysiol. *89*, 2778–2783.

Vogels, T.P., Sprekeler, H., Zenke, F., Clopath, C., and Gerstner, W. (2011). Inhibitory plasticity balances excitation and inhibition in sensory pathways and memory networks. Science *334*, 1569–1573.

Vogels, T.P., Froemke, R.C., Doyon, N., Gilson, M., Haas, J.S., Liu, R., Maffei, A., Miller, P., Wierenga, C.J., Woodin, M.A., et al. (2013). Inhibitory synaptic plasticity: spike timing-dependence and putative network function. Front. Neural Circuits *7*, 119.

Wang, R.A., and Randić, M. (1996). alpha-subunit of CaM-KII increases glycine currents in acutely isolated rat spinal neurons. J. Neurophysiol. *75*, 2651–2653.

Wehr, M., and Zador, A.M. (2003). Balanced inhibition underlies tuning and sharpens spike timing in auditory cortex. Nature *426*, 442–446.

Werthat, F., Alexandrova, O., Grothe, B., and Koch, U. (2008). Experience-dependent refinement of the inhibitory axons projecting to the medial superior olive. Dev. Neurobiol. *68*, 1454–1462.

Yamanaka, I., Miki, M., Asakawa, K., Kawakami, K., Oda, Y., and Hirata, H. (2013). Glycinergic transmission and postsynaptic activation of CaMKII are required for glycine receptor clustering in vivo. Genes Cells *18*, 211–224.

Yin, T.C., and Chan, J.C. (1990). Interaural time sensitivity in medial superior olive of cat. J. Neurophysiol. *64*, 465–488.

Yuste, R., and Bonhoeffer, T. (2001). Morphological changes in dendritic spines associated with long-term synaptic plasticity. Annu. Rev. Neurosci. *24*, 1071–1089.

STAR★METHODS

KEY RESOURCES TABLE

REAGENT or RESOURCE	SOURCE	IDENTIFIER
Experimental Models: Organisms/Strains		
Mongolian gerbil	Charles River Lab.	Strain code: 243
Software and Algorithms		
Custom macros for Igor Pro	WaveMetrics	6.37

CONTACT FOR REAGENT AND RESOURCE SHARING

Further information and requests for resources and reagents should be directed to the lead contact Nace Golding at golding@austin.utexas.edu.

EXPERIMENTAL MODEL AND SUBJECT DETAILS

Mongolian gerbils of both sexes aged 9-35 days we used. Animals were obtained from our own colony (of Charles River origin) or purchased from Charles River Laboratories. All animal procedures were approved by the University of Texas at Austin Animal Care and Use Committee in compliance with the recommendations of the United States National Institutes of Health.

METHOD DETAILS

Tissue preparation

To extract brain tissue, gerbils were decapitated under isoflurane anesthesia and the brain quickly removed in oxygenated ACSF at room temperature. For P9-20 gerbils our standard ACSF was used containing the following, in mM: 125 NaCl, 2.5 KCl, 1.5 $CaCl_2$, 1.5 $MgSO_4$, 25 $NaHCO_3$, 1.25 NaH_2PO_4, 25 dextrose, pH 7.40 with NaOH, ~310 mmol/kg. For P27-35 gerbils, sodium replacement cutting solution was used containing the following, in mM: 135 N-methyl-D-glucamine (NMDG, Sigma), 1.25 KCl, 1.25 KH_2PO_4, 0.5 $CaCl_2$, 2.5 $MgCl_2$, pH 7.40 with HCl, ~310 mmol/kg. For most experiments, the brainstem was isolated and sliced horizontally 200 μm thick using a vibrating microtome (VT1200S, Leica). For the isolation of inhibitory synaptic inputs from the MNTB and LNTB, coronal slices were made following a blocking cut behind the cerebral cortex. Slices were incubated in ACSF containing the following in mM: 110 NaCl, 2.5 KCl, 1.5 $CaCl_2$, 1.5 $MgSO_4$, 25 $NaHCO_3$, 1.25 NaH_2PO_4, 25 dextrose, 5 N-Acetyl-L-cystine, 5 Na-ascorbate, 3 Na-pyruvate, 2 thiourea, pH 7.45 with NaOH, continuously bubbled with 5% carbogen, ~310 mmol/kg at 35°C for 30 min. and then maintained at room temperature in the same incubation solution until being transferred to the stage for recordings in standard ACSF.

Electrophysiology

MSO principal cells were targeted using infrared differential interference contrast microscopy (Axioskop 2 FS Plus with 40x objective, Zeiss) and were selected based on their location in the tissue, shape, and responses to current steps (Scott et al., 2005). All recordings were made at 35 ± 0.1°C. Recordings were made using borosilicate pipettes with resistances of 2-7 MΩ (1.5 OD, Sutter Instruments), with smaller tips used for iLTP to reduce washout and dendritic patch experiments and larger ones for voltage-clamp experiments.

For current-clamp experiments, pipettes were filled with an internal solution containing the following (in mM): 115 K-gluconate, 4.42 KCl, 0.5 EGTA, 10 HEPES, 10 Na_2 phosphocreatine, ~45 sucrose, 4 Mg-ATP, 0.3 Na-GTP, pH 7.30 with KOH, ~305 mmol/kg. This solution had a chloride reversal potential of −90 mV and established a –10 mV liquid junction potential in our ACSF which was corrected. For experiments with BAPTA internal, K-gluconate was reduced to 51.38 mM and replaced with 15.90 mM BAPTA tetrapotassium (ThermoFisher). This solution established a –13 mV liquid junction potential which was corrected. For the voltage-clamp experiments testing glutamate co-release and GluN2B subunit block, the internal solution contained (in mM): 45 $CsMeSO_3$, 80 CsCl, 0.5, 1.8 $CaCl_2$, 5 EGTA, 10 HEPES, 10 Na_2 phosphocreatine, ~14 sucrose, 2 Mg-ATP, 0.3 Na-GTP, 1.46 QX-314 (Br, Tocris), 0.02 ZD 7288 (Tocris), pH 7.30 with CsOH, ~305 mmol/kg. This solution established a –5 mV liquid junction potential which was corrected. For developmental NMDAR assessment experiments this internal solution was used with the addition of tetraethylammonium (TEA, 10 mM) and 4-aminopyridine (4-AP, 5 mM).

Whole-cell recordings were made with either Dagan BVC-700A amplifiers or an Axopatch 700B amplifier (Molecular Devices). Electrical stimulation was carried out using a constant current stimulator (Digitimer). Data were low-pass filtered at 5 kHz, digitized with an ITC-18 (HEKA Instruments) at 50 kHz, and acquired to computer using custom macros for IgorPro (Wavemetrics).

For iLTP experiments, glass stimulating electrodes were placed between the MNTB/LNTB and the MSO. Stimulation intensity was adjusted to evoke stable IPSPs. Evoked IPSPs, comparable responses to simulated IPSCs (sIPSPs) injected via the recording electrode adjusted to a similar amplitude, as well as a square pulse adjusted to ~1.5 mV were monitored every 10 s for 10 min to establish a baseline prior to the induction protocol and for at least 34 min. thereafter. The induction protocol consisted of trains of brief (1 ms), step current injections just sufficient to drive AP firing at 200 Hz along with paired electrically evoked glycinergic IPSPs isolated with 15 μM NBQX or in some cases CNQX. Trains consisted of 100 pairings at 200 Hz, repeated 10 times at 10 s intervals (Figure 1A). The resting membrane potential was maintained at –60 mV throughout the recordings using small DC currents as necessary.

To unambiguously isolate inhibitory inputs from the MNTB and LNTB for glutamate co-release experiments, we used glutamate puffing to identify cell bodies for subsequent selective electrical stimulation. A standard patch pipette was filled with a solution containing (in mM): 125 NaCl, 2.5 KCl, 10 Glu (Na hydrate, Sigma), 3 HEPES, 1.24 Fast Green (FCF, Sigma), pH 7.30 with NaOH, ~305 mmol/kg. The pipette was placed on a modified electrode holder attached to a pressure pulse system (Pressure System IIe, Toohey Company). The pipette was maneuvered over the target nucleus until a response was elicited in the voltage-clamped MSO neuron. The puff duration was reduced and the tip repositioned successively until the smallest possible PSC was obtained. At this point, the puff pipette was switched to electrical stimulation and the intensity adjusted to obtain a small PSC with some failures. After recording the PSC at –60 and +35 mV (series resistance correction $\geq$ 60%) the bath was switched to ACSF containing strychnine (1 μM, Sigma) and gabazine (5 μM, Tocris) to block inhibitory synaptic transmission. In ~65% of trials, there was an underlying fast PSC that was not blocked, likely from an excitatory fiber of passage. These trials were discarded.

For NMDAR assessment experiments the standard ACSF was supplemented with strychnine (1 μM), gabazine (5 μM), NBQX (15 μM), and D-serine (100 μM, Sigma) and the amount of Mg^{2+} was varied from nominally 0 to 0.1 mM and then 1 mM, while maintaining Ca^{2+} at 1.5 mM. Cells were patched and the internal (see above) was allowed to equilibrate for 10 min before data collection. Stimulation intensities were adjusted to evoke small EPSCs without failures. Holding levels from –80 to 50 mV were tested sequentially at an interval of 7 s and repeated 5 times for each Mg^{2+} level then AP-V (50 μM, Tocris) was washed on to block NMDARs, which eliminated responses in all cases. Each solution was given 10 min to equilibrate before data collection. The average of 3 AP-V traces at each voltage level was subtracted before further analysis. The subtracted data were then smoothed in Igor Pro using a 17-point moving average before extracting the amplitudes and kinetics. Series resistances were less than 20 MΩ and were compensated at 85% with 25% prediction and 5 kHz bandwidth. Conductances were calculated for each cell using the equation: $G = I/(V-E_{rev})$ where I is the average peak current amplitude, V is the holding potential, and E_{rev} is the reversal potential calculated with a linear fit from –10 to +20 mV. Individual Boltzmann fits with the bottom held at zero were used to obtain G_{max} and normalize the conductances. Boltzmann fits of the group data were held at 0 and 1 for the minimum and maximum, respectively.

QUANTIFICATION AND STATISTICAL ANALYSIS

Means are presented ± standard error of the mean (SEM) and compared using two-tailed Student's t tests that were unpaired unless otherwise noted. Fits were performed using GraphPad Prism 7. Significance was assessed using an alpha level of 0.05. Error bars that are smaller than the symbol they are paired with were omitted.